Snow accumulation and ablation measurements in a mid-latitude mountain coniferous forest (Col de Porte, France, 1325 m alt.): The Snow Under Forest (SnoUF) field campaigns dataset

Jean Emmanuel Sicart[1], Victor Ramseyer[1], Ghislain Picard[1], Laurent Arnaud[1], Catherine Coulaud[1], Guilhem Freche[1], Damien Soubeyrand[1], Yves Lejeune[2], Marie Dumont[2], Isabelle Gouttevin[2], Erwan Le Gac[2], Frederic Berger[3], Jean-Matthieu Monnet[3], Laurent Borgniet[3], Eric Mermin[3], Nick Rutter[4], Clare Webster[5,6], Richard Essery[7].

[1] Univ. Grenoble Alpes, IRD, CNRS, Grenoble INP, IGE, 38000 Grenoble, France.
[2] CNRM UMR 3589, Météo-France/CNRS, Centre d'Études de la Neige, Grenoble, France
[3] Univ. Grenoble Alpes, INRAE, LESSEM, 2 rue de la Papeterie-BP 76, St-Martin-d'Hères, F-38402, France.
[4] Department of Geography and Environmental Sciences, Northumbria University, Newcastle upon Tyne, NE1 8ST, UK
[5] WSL Swiss Federal Institute for Snow and Avalanche Research SLF, Davos, Switzerland
[6] Department of Geosciences, University of Oslo, Norway
[7] School of GeoSciences, University of Edinburgh, UK

Correspondence to: Jean Emmanuel Sicart (jean-emmanuel.sicart@ird.fr)

Abstract. Forests strongly modify the accumulation, metamorphism and melting of snow in mid and high-latitude regions. Recently, snow routines in hydrological and land surface models have been improved to incorporate more accurate representations of forest snow processes, but model inter-comparison projects have identified deficiencies, partly due to incomplete knowledge of the processes controlling snow cover in forests. The Snow Under Forest (SnoUF) project was initiated to enhance knowledge of the complex interactions between snow and vegetation. Two field campaigns, during the winters 2016-17 and 2017-18, were conducted in a coniferous forest bordering the snow study at Col de Porte (1325 m a.s.l, French Alps) to document the snow accumulation and ablation processes. This paper presents the field site, instrumentation, and collection and post-processing methods. The observations include distributed forest characteristics (tree inventory, LIDAR measurements of forest structure, sub-canopy hemispherical photographs), meteorology (automatic weather station and an array of radiometers), snow cover and depth (snow poles transect and laser scan), and snow interception by the canopy during precipitation events. The weather station installed under dense canopy during the first campaign has been maintained since then and provides continuous measurements throughout the year since 2018. Data are publicly available from the repository of the Observatoire des Sciences de l'Univers de Grenoble (OSUG) data center at http://dx.doi.org/10.17178/SNOUF.2022.

1 Introduction

Around 20% of Northern Hemisphere snow overlaps with forest (e.g., Rutter et al., 2009), and sub-canopy snow cover is closely related to eco-hydrological processes. Forests strongly modify the accumulation, metamorphism and melting of snow, they intercept part of the precipitation, modify radiation fluxes and surface roughness, and reduce albedo and wind speed (e.g., Otterman et al., 1988; Pomeroy et al., 2008; Musselman et al., 2012; Essery, 2013). For example, the model inter-comparison project SnowMIP2 (Essery et al., 2009; Rutter et al., 2009) evaluated 33 forest snow models differing in both process complexity and canopy implementation approaches. Major deficiencies of modeling snow in forests were identified, and the project concluded that model performance was limited by incomplete knowledge of the processes controlling snow cover in forests. Since then, numerous measurement campaigns have been conducted (e.g., Webster et al. 2016, 2018; Malle, et al., 2019; Mazzotti et al., 2019; Hojatimalekshah et al., 2021) and snow routines in hydrological and land surface models have been enhanced to incorporate more accurate representations of forest snow processes (e.g., Ellis et al., 2013; Gouttevin et al., 2015; Boone et al., 2017; Mazzotti et al., 2020). However, these improved routines still represent canopy as one homogeneous layer without accounting for the effects of vertical canopy heterogeneity on snow accumulation and ablation processes. Detailed snow and meteorological measurements are therefore still required, and remain an important step to better understand the complex interactions between snow and vegetation. Col de Porte (CDP) is a mid-elevation site located at 1325 m altitude (45.295°N, 5.766°E) in the Chartreuse mountain range in France, with a meadow bordered by a coniferous forest. The CDP meadow site has been operated by CEN-MeteoFrance with daily measurements of snow depth, air temperature, and precipitation recorded since 1960 (Lejeune et al., 2019; Morin et al., 2012). Hourly measurements of meteorological and snow variables required to run and evaluate detailed snowpack models such as Crocus (Vionnet et al., 2012) started in 1987 and have been almost continuous during the snow seasons since 1993. CDP is part of several observation networks at the national scale (e.g., Observation pour l'Experimentation et la Recherche en Environnement CryObsClim and Systèmes d'Observation et d'Expérimentation au long terme pour la Recherche en Environnement des glaciers, GlacioClim) and at the international scale (e.g., ILTER European Research Infrastructure, WMO Global Cryosphere Watch CryoNet network, GEWEX INARCH). For more details, the reader is referred to Lejeune et al. (2019). Only a few studies have investigated the snow cover distribution in the forest of CDP (e.g., Durot, 1999); however, the immediate proximity of the forest parcel to the historical, long-term open-area snow observatory of CDP offers a good opportunity to understand and relate the sub-canopy meteorological and snow processes to their open-area counterparts.

Two field campaigns have been conducted in the conifer forest bordering the reference meadow site to document the snow accumulation and ablation processes: from 16 January 2016 to 21 March 2017 and from 1 December 2017 to 15 March 2018. This paper presents the measurement methods that were applied in the forest plot during these two field campaigns. The observations include distributed forest characteristics (tree inventory, LIDAR measurements of forest structure, sub-canopy hemispherical photographs), meteorological variables (automatic weather station and an array of radiometers), snow height and water equivalent (snow poles transect and laser scan), and transects of snow interception by the canopy during precipitation events. The dataset also includes continuous measurements from the weather station in the forest from March 2018 to June 2022. Complementing the datasets, the repository of the Observatoire des Sciences de l'Univers de Grenoble data center also includes technical information, photographs and a detailed plan of the instrumentation.

2 Site and forest description

2.1 Site

The study site is a triangular forest parcel of 2000 m^2 (Figure 1) next to the meadow where the historical open-area snow measurements are conducted. It is delimited by a fence along its south and northeast sides. Its west side corresponds to the edge between the forest and the open meadow area. The terrain slope is around 10° oriented toward east-north-east. The stand is dominated by Norway spruce (*Picea abies*) with young silver firs (*Abies alba*). Some broadleaved trees are located along the west edge. The parcel exhibits two gaps in the canopy. The smaller one is in the south-west, while the larger one is at the center and extends toward the south fence (Figure 2). During the first campaign, the annual maximum snow depth was around 100 cm in the open site (meadow reference site) and only around 50 cm under the canopy. During the second campaign, the annual maximum snow depth was around 160 cm in the open site and 130 cm under the canopy.

Figure 1: Aerial photographs of the site taken on 30 August 2016, with locations of the sensors during the 2017-18 field campaign. On the left is the meadow with part of the long-term instrumentation for the Col de Porte site. Labels “2” and “3” refer to sensors SW2 and SW3.

2.2 Forest measurements

2.2.1 Manual forest inventory

An inventory of trees higher than 1.3 m took place during field campaigns between September 2016 and July 2018. On 13-14 September 2016, live and dead trees were inventoried, and the following observations and measurements were performed:

- diameter at breast height (DBH, measured with a tape measure at 1.3 m height above the ground, upslope of the tree);
- species;
- tree height measured with a Haglöf Vertex 4 hypsometer, only for trees with a DBH larger than 7.5 cm.

Tree identification numbers were painted on the trunk at a height around 1.3 m above ground. Three reference poles were positioned in the site and geolocated using a Trimble GeoExplorer 6000 XH GNSS receiver. Trees were mapped relative to a nearby pole by measuring the ground distance (Vertex 4 hypsometer), slope (clinometer) and azimuth (compass). Tree position precision relative to the reference pole is expected to be better than 50 cm, whereas GNSS precision under the forest canopy is of the order of a few meters. In total, 141 trees were inventoried, including 128 live trees, 3 dead trees and 10 stumps.

On 5 May 2017, vertical crown projections of live trees with a DBH larger than 7.5 cm were measured following the method specified by Rohle (1986) but using a clinometer instead of a plummet to locate the crown extension. The horizontal distances between the trunk center and the vertical projection of the furthest live branch along north, south, east and west directions were measured with a tape. If several tree stems were sprouting from a common base, the whole clump was considered to have one single crown and its extension was measured from the stem with the largest diameter in the clump. On 20 June 2017, tree positions were measured with a Leica TS02 total station located in the open area at the west of the forest. The total station position was recorded with a Trimble R2 differential GNSS receiver, ensuring centimetric accuracy. On July 25, 2018, heights and crown extensions were measured on trees with a DBH smaller than 7.5 cm (Table 1). The tree inventory was extended outside the southern fence to include trees which might cast shadows inside the forest parcel (DBH, height, crown extension, species). Their positions were measured with slope (clinometer), azimuth (compass) and ground distance (Vertex 4 hypsometer) relative to a reference pole located with a GNSS receiver.

Table 1: Tree inventory on July 25, 2018

Species	Health status			
	Standing, live	Standing, dead	Cut between June 2017 and July 2018	Large stump (cut before Sept. 2016)
Abies alba	54	2	0	0
Picea abies	52	1	0	10
Sorbus aucuparia	20	0	1	0
Acer pseudoplatanus	15	0	1	0
Fagus sylvatica	4	0	0	0
Fraxinus excelsior	1	0	0	0

Tree easting and northing values in the RGF 93 - Lambert 93 projected coordinate system were then derived from the total station coordinates if available, or from their polar coordinates relative to a reference pole. Tree altitude values were computed from the airborne laser scanning data (see Section 2.2.2) by bilinear interpolation of the ground-classified points at the location of trees. Figure 2 shows a map of inventoried live trees and canopy heights. In the forest stand inside the fence, most of the trees are between 30 and 40 m high (Figure 3) and the total basal area is about 66.3 m^2/ha. It includes 52 firs, 43 spruce and 33 broadleaved trees. Trees measured outside the southern fence included 9 spruce, 2 firs and 7 broadleaves. Tree position accuracy is estimated to be better than 10 cm for the trees measured with the total station inside the fenced area and around 50 cm for additional trees outside the fence. Luoma et al. (2017) reported a precision of 0.5 m (standard deviation) for height measurements with a Vertex 4 clinometer. Elzinga et al. (2005) reported a standard deviation of 0.5 cm for diameters measured with a tape measure. Measurement errors on crown extension is mostly due to the difficulty of assessing the vertical projection of the branches' extent on the ground. Accuracy is expected to be from 10 cm for small trees (height smaller than 4 m) to 50 cm for the tallest ones (around 30 m).

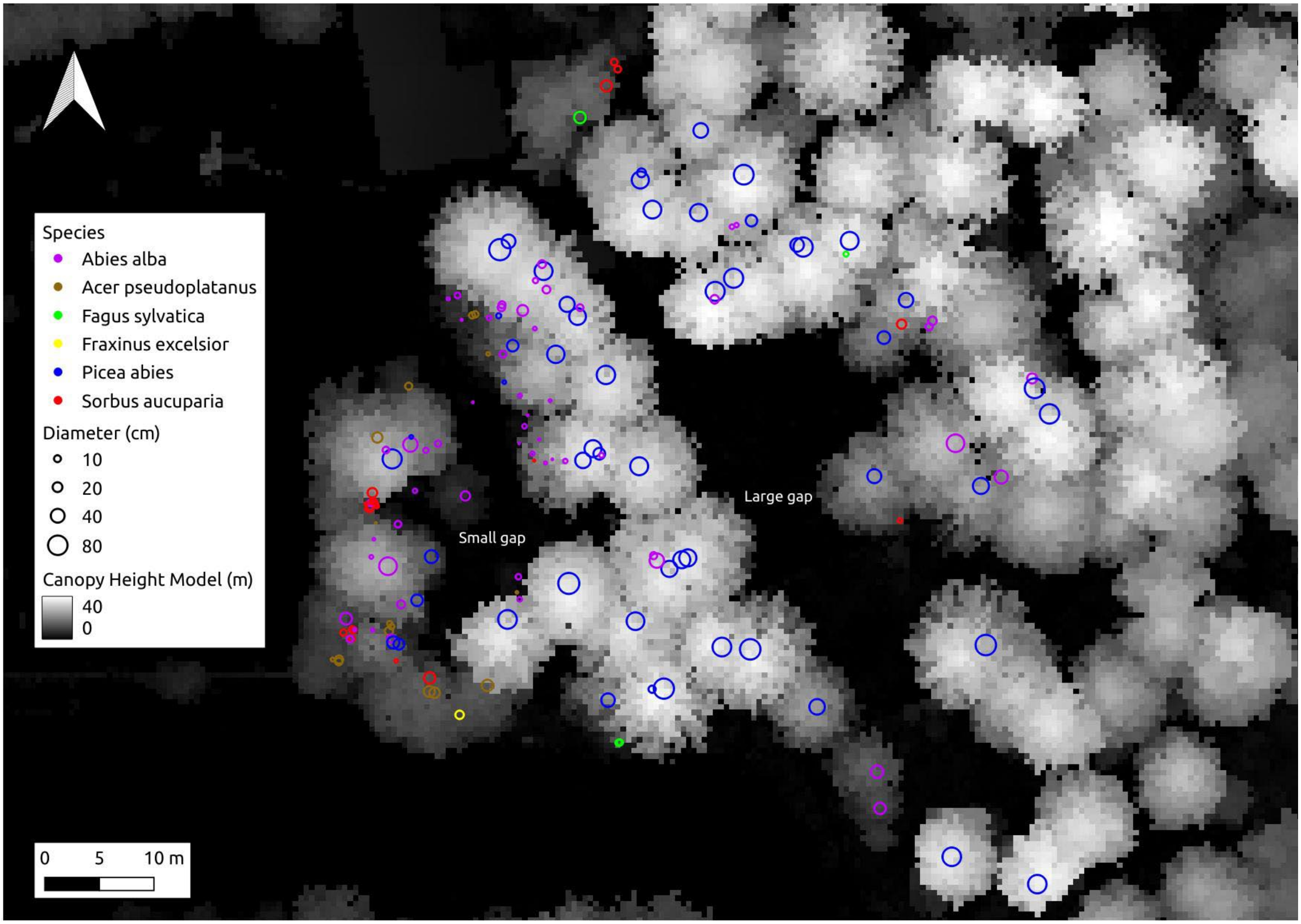

Figure 2. Map of inventoried live trees (2016-2018 campaigns) and canopy height model derived from airborne laser scanning acquired between 30 August and 2 September 2016.

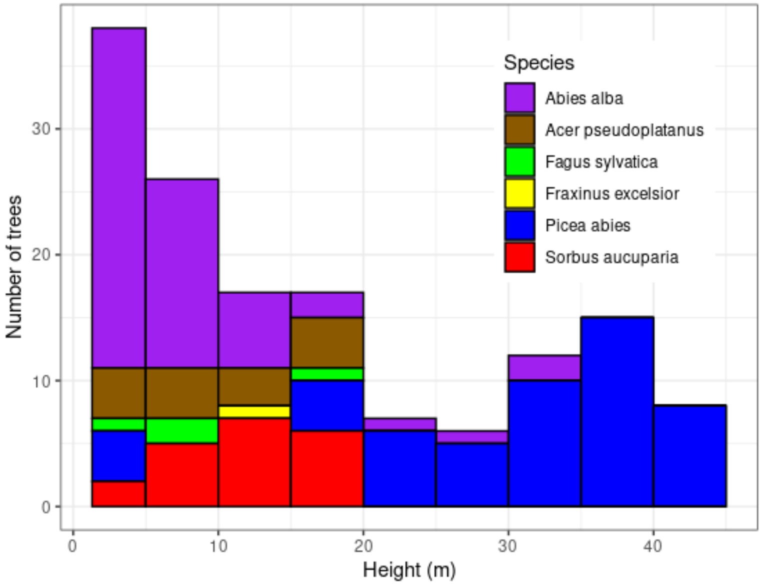

Figure 3: Height distribution of living trees taller than 1.3 m (2016-2018 campaigns).

2.2.2 Airborne remote sensing measurements

Airborne laser scanning (ALS) is a remote sensing technique based on LiDAR that can provide a 3D point cloud of forest structure. The point cloud can be processed to derive forest metrics used to parametrize snow interception, such as leaf area index or canopy closure (e.g., Helbig et al., 2020). ALS was acquired during a campaign covering 123.5 km^2 (which integrates the Col de Porte site) between 30 August and 2 September 2016, using a Riegl LMS Q680i sensor mounted on a helicopter. The scheduled flight height and speed were 750 m above ground and 70 knots, respectively. The scan frequency was 300 kHz with a scan angle of ± 30°. The aircraft trajectory was computed from the Inertial Measurement Unit and GPS data. Point coordinates were extracted and computed using the RiAnalyse and RiWorld software (http://www.riegl.com/products/software-packages/). The point cloud was then classified as ground/non-ground using Terrasolid (https://terrasolid.com/). To assess the accuracy of elevation measurements, 318 ground control points were measured with differential GNSS in 11 flat, vegetation-less plots. Differential GNSS horizontal accuracy is around 2-3 cm in such areas. Comparison of the control points with the point cloud yielded an altitudinal accuracy of 4.7 cm (root mean square error of differences), with a bias of -0.3 cm. The point cloud was delivered as tiled files in LAS format, which is the most common format for LiDAR point cloud exchange and is maintained by the ASPRS[1] . The coordinate system was RGF 93 - Lambert 93, with altitude in the system NGF-IGN69. The point cloud extracted on a 200 m radius disk centered on the study site was exported in a single compressed LAS file (v1.1

---

[1] https://www.asprs.org/divisions-committees/lidar-division/laser-las-file-format-exchange-activities

format 1). Pulse density in the study site is 17 points/m^2, resulting in densities of 3.3 points/m^2 for ground points and 28 points/m^2 with multiple returns for canopy points.

For the extent of the inventoried trees plus a 30 m buffer, digital surface models were computed at 0.5 m resolution from the ALS point cloud. The digital terrain model (DTM) was computed by estimating the altitude of each cell center by bilinear interpolation of ALS points classified as ground. The point cloud was normalized by subtracting the ground altitude at the position of each point, estimated by bilinear interpolation of ground points. A canopy height model (CHM) was computed by retaining the highest value of normalized heights in each cell. Cells without values were filled by the median of their 3×3 neighborhood. The DTM and CHM were delivered as raster files in tif format. Aerial photographs were also taken during the ALS acquisition. Pictures were used to produce a 10 cm resolution RGB orthophoto provided as a tif file for the extent of the DTM. Figure 4 shows a perspective view of the 3D point cloud acquired by the airborne laser scanning.

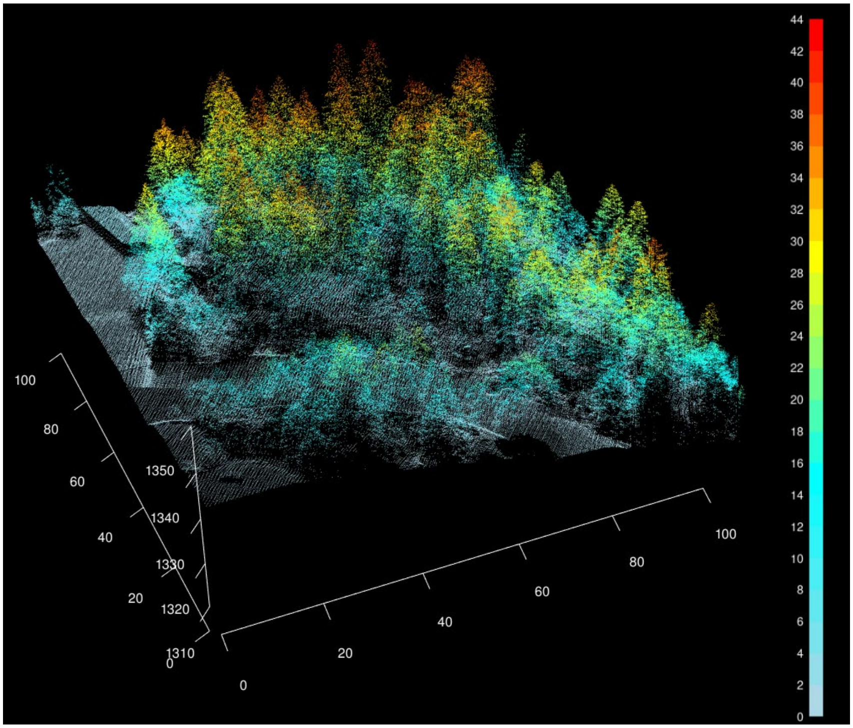

Figure 4: Perspective view of the 3D point cloud of the area of interest acquired by airborne laser scanning between 30 August and 2 September 2016. Points are colored according to their height above ground.

2.2.3 Hemispherical photographs

Hemispherical photographs were taken on 4 September 2017 at each radiometer location. Although the sky was not completely overcast, there was no direct sunlight. A Nikon Coolpix 4300 digital camera was used with a Nikon FC-E8 fisheye lens, mounted 60 cm above the ground surface on a tripod. The camera was aligned to north with a compass and carefully levelled using a bubble level. All sites were snow-free when the hemispherical photographs were taken. Sky view factors were then calculated following Essery et al. (2008) assuming an equiangular lens projection. To distinguish vegetation from sky pixels, and to calculate the sky view factor at each location, a brightness threshold was selected manually for each hemispherical photograph (Figure 5). This allows us to account for variations in illumination conditions during changes in cloud cover or thickness. Brightness thresholds can be selected automatically (Nobis and Hunziker, 2005), but the manual process gave a clear distinction between canopy and sky pixels in every case here. Calculated sky view factors ranged from 0.15 to 0.35 at the radiometer sites, which were mostly situated under a rather dense canopy. Reid et al. (2014) estimated the uncertainty in the sky view factor using this method to be ±0.02.

Figure 5: Example of a hemispherical photograph (left) and a binary image (right, white pixels are sky and black pixels are canopy, calculated sky view factor 0.25). The photograph was taken on 4 September 2017 at radiometer A1 (Figure 1).

3 Meteorological and snow observations in the forest

3.1 Radiometer array

An array of 15 CMP3 Kipp & Zonen pyranometers and 11 CGR3 Kipp & Zonnen pyrgeometers was deployed on the snow surface from dense canopy to an opening (Figure 1). During the first campaign, each radiometer was positioned horizontally with a bubble level on a wooden board placed on the snow surface. During the second campaign, the horizontal support of the radiometers was attached to a vertical bar fixed in the ground. The height of the support (10-20 cm) was adjusted to the snow surface every two or three days. This system allowed better stability and levelling of the radiometers. One-minute averages of the incoming radiation fluxes measured at five second time intervals were recorded by two Campbell Scientific CR3000 data loggers. Inter-calibration of the sensors before the campaigns led to estimates of sensor accuracies close to those announced by the manufacturer: ± 12 W m^{-2} for solar radiation and ± 8 W m^{-2} for longwave radiation, in accordance with uncertainty estimations from similar sensors (Halldin and Lindroth 1992, Philipona et al. 2001, Michel et al. 2008, Van den Broeke et al. 2004). The radiation data were carefully post-processed to remove periods when the sensors were snow covered or tilted.

3.2 Weather station

The weather station was installed under rather dense canopy (sky view factor ~ 0.2) during the first campaign and has been maintained since then. Table 2 lists the sensors installed on the station, their specifications and their accuracy according to the manufacturers. The ultrasonic depth gauge measures the snow height. Ten temperature probes buried in the ground are used to estimate the heat conduction flux. 15-minute averages of the data measured at 10 second time intervals are recorded by a Campbell Scientific CR3000 data logger. An AXIS M1125-E camera took pictures of the surface around the weather station every three hours during daytime. These images were used to monitor surface and sensor conditions. A Campbell Scientific IR120 infrared sensor was used to measure the surface temperature of a trunk close to the meteorological station (Figure 1). One-minute averages of longwave irradiance measured at five second time intervals were recorded by a Campbell Scientific CR1000 data logger.

Table 2: Variables measured by the weather station below the canopy along with the sensor type, heights and precision according to the manufacturers.

Quantity	Sensor Type	Height (cm)[1]	Accuracy according to the manufacturer
Air temperature, °C, and relative humidity, %	Campbell CS215C	210	±0.2°C ±2% in [0-90%] ±3% in [90-100%]
Wind speed and direction, m s^{-1} and degrees	Gill windsonic	210	±0.3 m s^{-1} ±3 degrees
Incident and reflected short-wave radiation, W m^{-2}	Kipp & Zonen CM3 $0.3<\lambda^2<2.8$ µm	100	±10% for daily sums
Incoming and outgoing long-wave radiation, W m^{-2}	Kipp & Zonen CG3 $5<\lambda<50$ µm	100	±10% for daily sums
Surface elevation changes, mm	Ultrasonic depth gauge Campbell SR50	180	±1 cm
Temperature in the ground, °C	108 Campbell	-2.5, -8, -15, -30, -60[3]	≤ ±0.01°C

[1] height above snow-free ground

[2] spectral range in wavelength

[3] two sensors for each depth

As an example of the use of these measurements, Figure 6 shows hourly changes in air and soil temperatures and snow depth from December 2018 until June 2019, a winter characterized by deep and sustained snow cover. Snow cover began to build in late December, reaching a maximum of 90 cm in early February. Melt rates became significant as air temperatures remained consistently above 0°C through late February. Snow cover disappeared by the end of March, although there were a few snowfalls through May. Snow cover strongly affected soil temperatures to a depth of 60 cm. The disappearance of the main snow cover at the end of March suddenly reversed the temperature gradient in the soil (the deeper soil became colder than the surface). Soil temperatures were also affected by a few snowfalls in April, associated with short periods of cold weather.

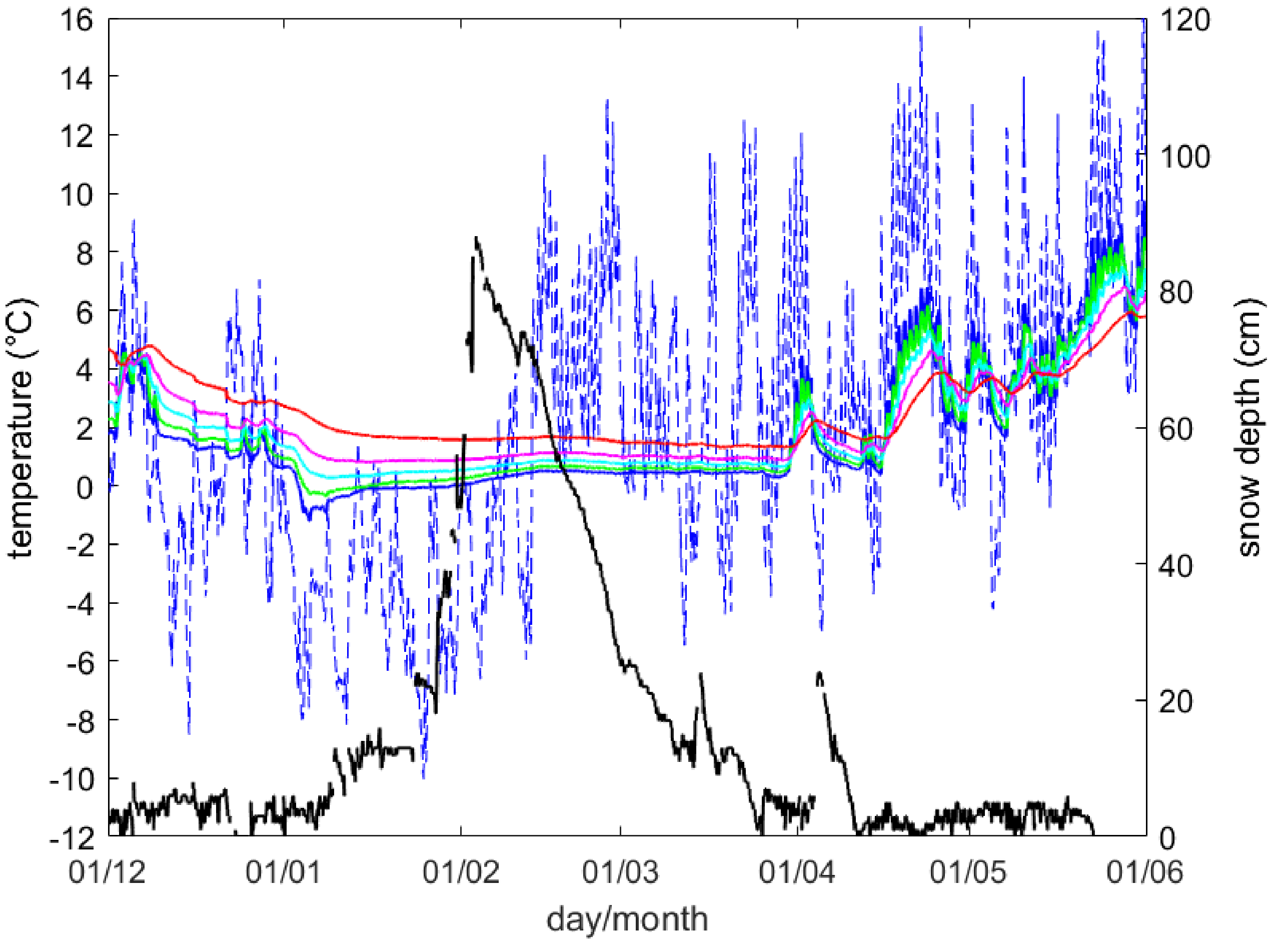

Figure 6: Left axis: air temperature (blue dotted line) and soil temperature at 2.5, 8, 15, 30 and 60 cm depth (blue, green, cyan, magenta and red solid lines, respectively). Right axis: snow depth (black line). Hourly data from the weather station in the forest (Table 2) from 1 September 2018 to 1 June 2019. The data gaps in the snow depth time series are mainly due to snowfall events that disrupted the measurements.

3.3 Snow measurements

In order to document the spatial variability of snow cover in the forest, a transect of 18 snow poles was deployed in early winter 2016-2017 (Figure 1). The locations of these snow poles (spaced 2 m apart) were georeferenced in Lambert 93 coordinates. For each pole, the snow depth was measured approximately every two weeks during the two field campaigns. Snow water equivalent measurements were carried out every week for only four poles at a time, alternating among the 18 poles to minimize destruction of the local snowpack structure. Detailed studies by Morin et al. (2012) and Lejeune et al. (2019) estimated the uncertainties in snow depth and snow water equivalent measurements to be ± 1 cm and ± 5 %, respectively, in agreement with the estimation of López-Moreno et al. (2020) derived from a comparison of measurements with different snow core samplers. Simultaneously, measurements of snow depth and water equivalent were made in the reference meadow site as described in Lejeune et al. (2019).

3.4 Precipitation tanks

The amount of snow held in the canopy can be large and remains difficult to measure. Due to the sublimation of intercepted snow, a large portion of the snow retained in the canopy never reaches the ground, and the interplay of interception, sublimation and delayed deposition on the ground creates significant below-forest heterogeneity in snow accumulation (e.g., Helbig et al., 2020). To try to measure snow interception by the canopy, 24 "precipitation tanks" (1 m x 0.39 m) were built and then deployed under the canopy in three eight-meter transects at the start of winter 2017-2018 (Figures 1 and 7). Snow was taken from the precipitation tanks and weighed after each of the seven significant snowfall events between 20 February and 3 April 3 2018. The uncertainties in this new measurement method developed by CEN-MeteoFrance are difficult to estimate. Vincent (2018) estimated the measurement uncertainty at about 5%, but additional studies are needed.

Figure 7: Precipitation tanks installed below the canopy (photograph by Y. Lejeune).

3.5 Rugged Laser Scan

The Rugged Laser Scan (RLS) is a scanning laser meter that was installed at about 4 m above the ground close to the center of the main clearing to monitor spatio-temporal variations of snow depth under various canopy covers on a daily or two-daily basis (Figure 1). The device is described in detail in Picard et al. (2016) and is specially designed to monitor snow heights. It comprises a laser meter mounted on a 2-axis stage and can scan ≈ 200000 points in 4 hours. The laser meter was used in scan mode. With a setup at 4 m height, and azimuth angles varying from -90° to +90° (azimuth angle 0° points towards 225° (south-west)) and zenith angles varying from 19° and 62°, the scanned area is a half-disk of radius ~7 m, with a surface area of about 80 m^2. The area encompasses three pairs of radiometers installed on the snow surface. Data acquired by the laser meter for a given day are processed to build a cloud of x, y, z points, which is then interpolated and averaged on a regular 3 cm grid. The grid is common to all measurement days so it is easy to compare the evolution of the snow surface. The vertical precision was evaluated to be about 3 mm and the accuracy to be 1 cm (Picard et al. 2016).

The RLS was operated during the two field experiments. The first season was from 22 February 2017 to 4 April 2017 (42 days) and had 42 valid acquisitions (once a day). The second season was from 5 December 2017 to 11 March 2018 (160 days) and had 81 valid acquisitions because scans were scheduled every other day during the winter (accumulation period) and every day during the melt season. Figure 8 shows an example of snow depths on 15 April 2018 and Figure 9 shows the changes in daily spatial averages of the snow depth during the 2017-18 field campaign.

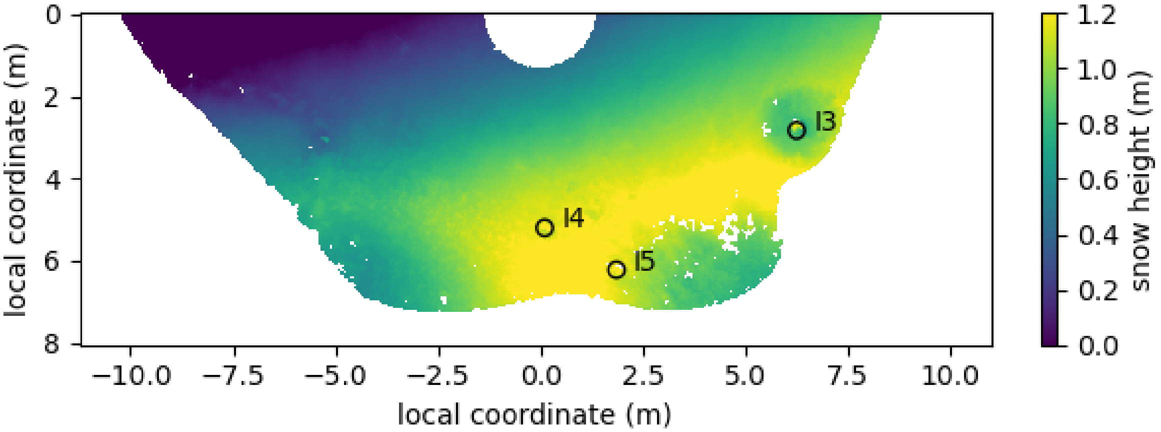

Figure 8: Snow height (m) derived from the digital terrain models (DTM) measured by the rugged Laserscan, obtained by subtracting the snow-free DTM from the 15 April 2018 DTM. The measurement area encompassed three radiometers (I3, I4 and I5).

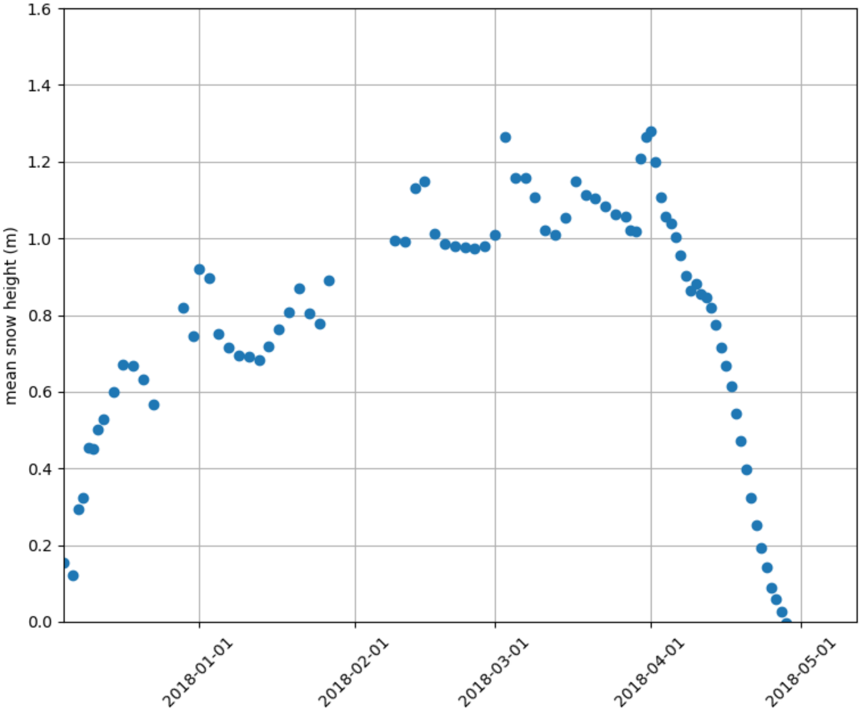

Figure 9: Daily spatial averages of the snow depth measured by the rugged Laserscan during the 2017-18 field campaign.

4 Spatial variability, measurement uncertainties and data validation

This section provides estimations of the dataset uncertainties related to measurement uncertainties and spatial variability of the variables within the measurement plot. The uncertainties of the sensors and the measurement methods have been described in the previous sections. For meteorological measurements, sensor manufacturers generally provide reliable information on sensor accuracy (Table 2). In this Section, comparisons of radiation, air temperature, and snow measurements at different locations provide a better insight into the measurement uncertainties and a first validation of the data set.

Figure 10 illustrates the spatial variability of the incoming shortwave and longwave radiation fluxes below various forest covers. It shows the effects of clouds and canopy cover on the sub-canopy 15-minute radiation fluxes during an overcast day and a clear sky day of the 2017 campaign. Under thick cloud cover (January 31), shortwave radiation, mostly diffuse, reaching the ground remains small but steadily increases with decreasing canopy cover (increasing sky view factor). Sky and vegetation were characterized by similar temperatures and longwave emittance (close to 1), and all the pyrgeometers recorded similar longwave radiations fluxes (within a few W m^{-2}, confirming the good accuracy of the sensors), without relation to the canopy cover. In clear sky conditions (February 18), shortwave irradiance is mostly direct. Sunflecks on the ground below the canopy caused peaks of shortwave irradiance of various amplitudes and at different times at the different pyranometers, superimposed on the diffuse shortwave radiation that has penetrated through the canopy. The diurnal changes of sub-canopy longwave irradiance are remarkably parallel between the different measurement sites. The constant offset between the signals is related to the canopy cover due to the large contrast between the large emittance of vegetation and the small emittance of clear, cold sky; the larger the sky view factor, the smaller the longwave irradiance (Figure 10d).

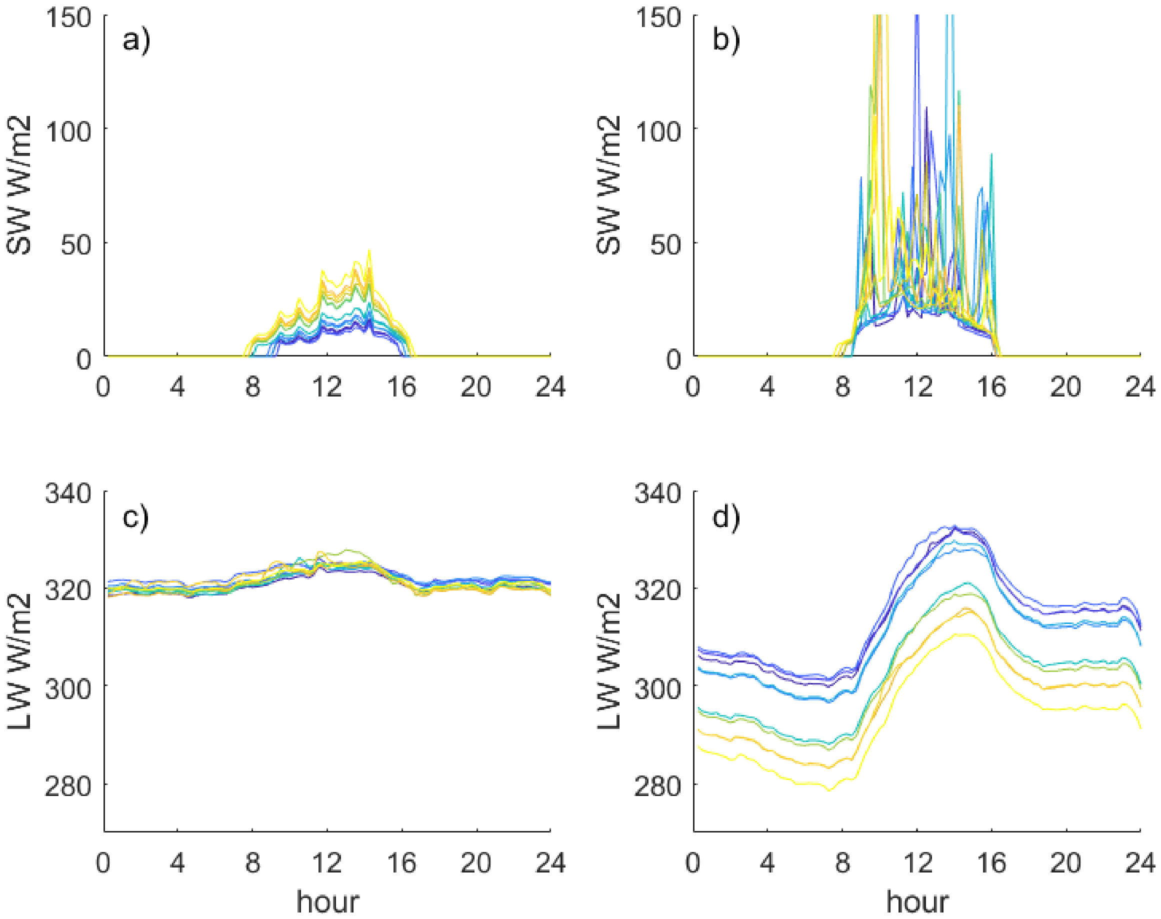

Figure 10: Shortwave (a, b) and longwave (c, d) incoming radiation fluxes measured by each radiometer during an overcast day (January 31: a, c) and during a clear-sky day (February 18: b, d). 15-minute averages of the sub-canopy fluxes during the 2017 campaign. Line color is related to the sky view factor V_f from dark blue (lowest $V_f = 0.17$) to yellow (highest $V_f = 0.32$).

Figure 11 illustrates the hourly air temperature differences between forest and meadow. During daytime, the forest is generally a few degrees colder than the open meadow site, with the difference increasing on clear sky days when the air is warmest (high

T_{open}). During the night, the forest is generally slightly warmer than the meadow, with the difference reaching a few degrees on cold clear-sky nights (low T_{open}). Thus, average daily air temperatures are quite similar in the forest and meadow site ($dT \sim$ 0.2°C on average during the 2018 campaign) because warmer nights counterbalance cooler days in the forest relative to the meadow. In addition, warmer cloudy periods tend to counterbalance cooler clear-sky periods in the forest relative to the meadow.

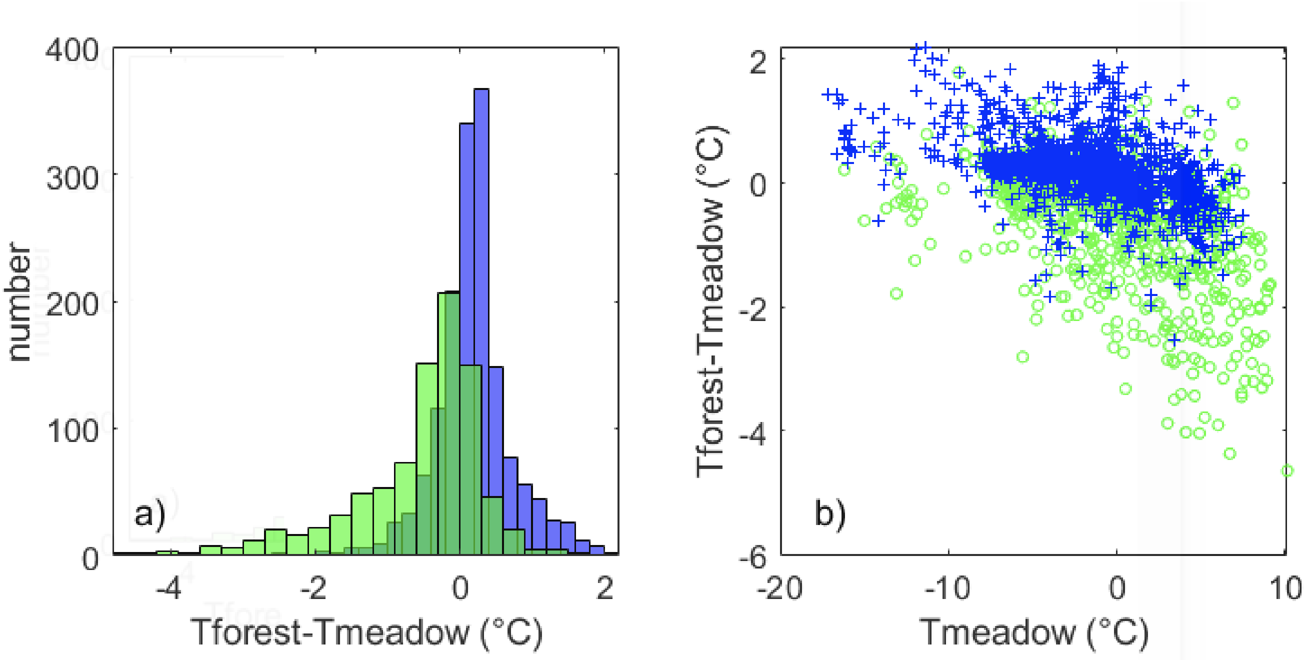

Figure 11: Difference of hourly air temperature between forest and meadow (T_{forest}-T_{meadow}) during the 2018 campaign. (a) shows histograms, (b) shows (T_{forest}-T_{meadow}) according to T_{meadow}. The distinction between daytime (green bars and circles) and nighttime (blue bars and crosses) values is based on a threshold on the shortwave incoming radiation fluxes in the meadow site ($SW < 10$ W m^{-2} during nighttime).

Figures 12 and 13 illustrate the spatial variability of snow depth and snow water equivalent measurements in the open meadow and along the snow pole transect in the forest (see locations in Figure 1) during the 2017 and 2018 field campaigns. As previously mentioned, snow cover lasted several weeks longer and was deeper in the second campaign than in the first, reaching a maximum in the meadow of 160 cm and 100 cm, respectively. The seasonal maximum snow depth under the canopy was smaller than that of the meadow by factors ranging from 0.20 to 0.75, depending on the local canopy cover. For the snow water equivalent, these ratios ranged from 0.16 to 0.60. Relative decreases in snow depth and water equivalent in the forest transect compared to the meadow were greater during the first campaign characterized by shallow snow cover. Figures 12 and 13 suggest that the effects of the forest on snow cover are more marked during the winter accumulation season (likely due to interception of snow by the canopy), whereas melt rates during the short ablation season appear to be quite similar in the forest and the meadow. Snow generally disappears earlier in the forest than in the open meadow, but differences in the duration of snow cover are generally small, except in years of low snowfall, and highly location-dependent due to the high spatial variability of snow depth in the forest (Figures 12 and 13). This is in line with the meta-analysis of Lundquist et al. (2013) for a dense forest site in a mild climate, but further analysis of snow and meteorological data is needed to investigate this issue at Col de Porte.

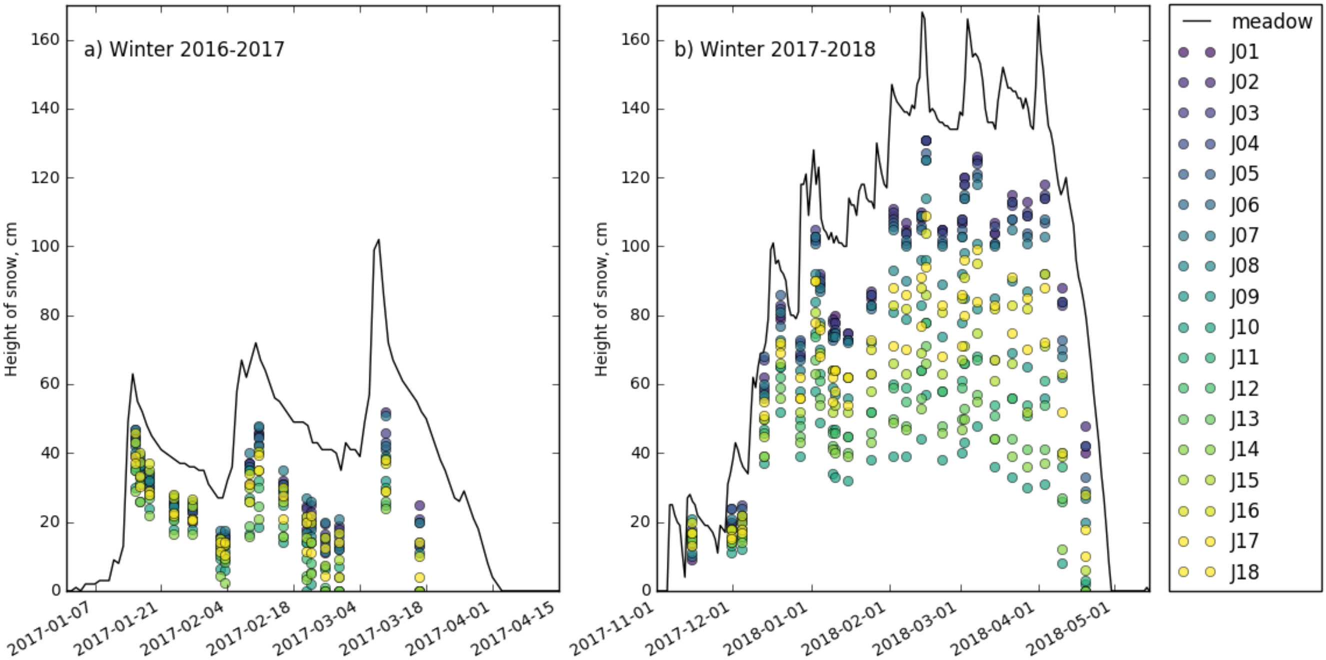

Figure 12: Reference snow depth measured in the meadow from Lejeune et al., 2019 (black line) and manually measured at the snow pole transect in the forest (circles, each color corresponds to a snow pole, Figure 1) during the 2017 (a) and 2018 (b) field campaigns.

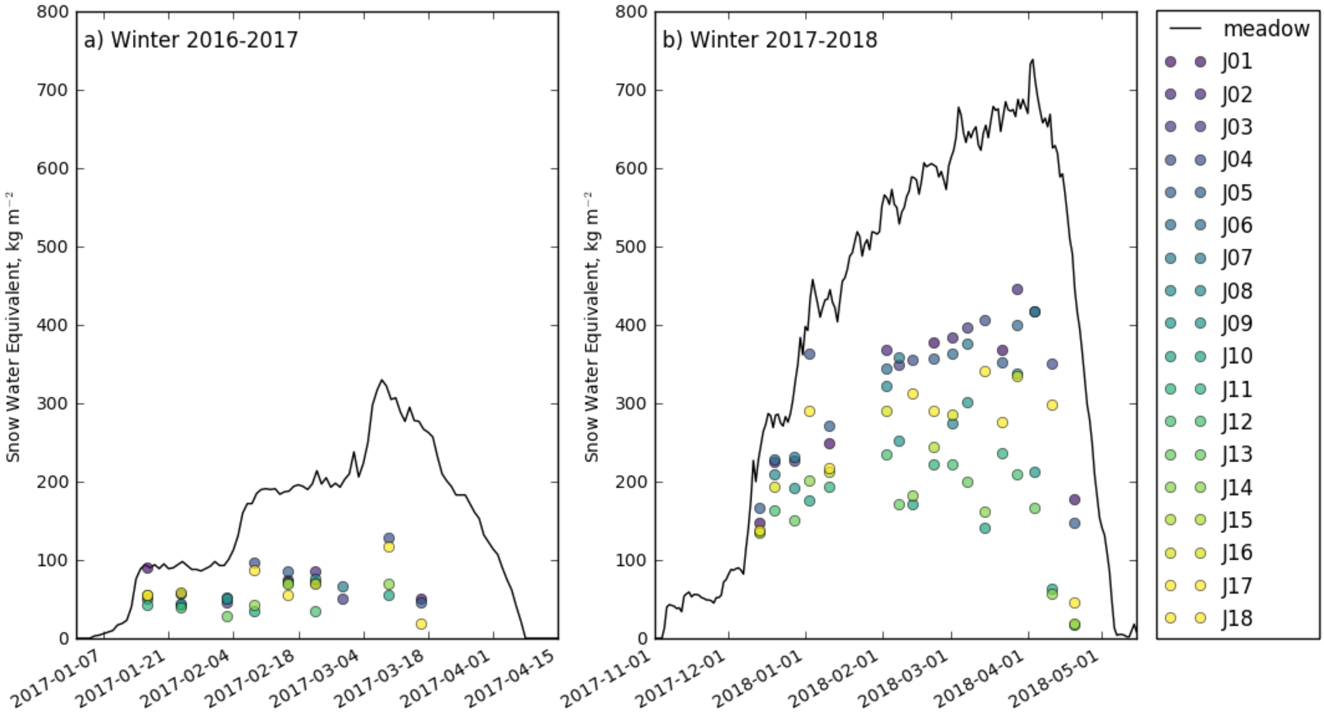

Figure 13: Reference Snow Water Equivalent measured in the meadow site with a cosmic ray neutron sensor (black line, see details in Lejeune et al., 2019) and manually measured at the snow pole transect in the forest (circles, each color corresponds to a snow pole, Figure 1) during the 2017 (a) and 2018 (b) field campaigns.

5 Conclusions

The datasets collected in the Col de Porte coniferous forest will allow research on the effects of the canopy on snow accumulation and ablation processes under different canopy covers. Two intensive field campaigns were conducted during the winters of 2016-17 and 2017-18 and an automatic weather station has been maintained under the canopy since then. Meteorological and snow measurements (automatic weather station, radiometer array, snow pole transect, laser scan, precipitation tanks to estimate snow interception by the canopy) were complemented by canopy observations (tree inventory, LIDAR measurements of forest structure, sub-canopy hemispherical photographs). Continuous measurements throughout the year at high temporal frequency (15-minute) from the meteorological station allow hydrological and ecological studies related to seasonal changes in micrometeorological and soil conditions.

Data availability

All datasets described and presented in this paper can be openly accessed from the repository of the Observatoire des Sciences de l'Univers de Grenoble (OSUG) data center at: http://dx.doi.org/10.17178/SNOUF.2022 (Sicart et al., 2022). Table 3 provides the links to the different datasets.

Table 3: Links to the dataset repository.

Data set	Period	Format	Repository
Forest inventory	13-14 September 2016 27 July 2018	csv	https://doi.osug.fr/data/public/SNOUF/forest/
Hemispherical photographs	4 September 2017	png	https://doi.osug.fr/data/public/SNOUF/hemis-photos/
Rugged laser scan	22 Feb to 4 April 2017 5 Dec 2017 to 13 May 2018	netCDF	https://doi.osug.fr/data/public/SNOUF/laser-scan/
Airborne laser scanning	30 August and 2 September 2016	laz	https://doi.osug.fr/data/public/SNOUF/lidar/
Weather station and radiometer array measurements	16 Jan 2016 to 14 June 2022	csv	https://doi.osug.fr/data/public/SNOUF/meteo/
Snow pole and precipitation tank measurements	16 Jan 2016 to 21 March 2017 1 Dec 2017 to 15 March 2018	xlsx	https://doi.osug.fr/data/public/SNOUF/snow/

Author contributions

JES organized the data and wrote the first draft of the manuscript. JMM and YL cleaned and corrected the forest and snow measurements, respectively. LA and GP cleaned and corrected the laser scan measurements. VR and DS analyzed the meteorological data. All authors participated in the field campaigns, collected and assembled data records, and contributed to writing the paper.

Competing interests

The authors declare that they have no conflict of interest.

Disclaimer

Any reference to specific equipment types or manufacturers is for informational purposes and does not represent a product endorsement.

Acknowledgments and funding

This project was conducted within the grant Labex OSUG@2020 ANR10 LABX56 UGA and with financial support from the IGE and the CEN, through a collaboration between the French institutes IGE, CEN and INRAE, and the universities of Edinburgh and Northumbria in the UK. Marie Dumont has received funding from the European Research Council (ERC) under the European Union's Horizon 2020 research and innovation program (IVORI; grant no. 949516). We thank Laurent Bourges (CNRS, OSUG) for his support in managing the dataset.

References

Boone, A., Samuelsson, P., Gollvik, S., Napoly, A., Jarlan, L., Brun, E., and Decharme, B.: The interactions between soil-biosphere-atmosphere land surface model with a multi-energy balance (ISBA-MEB) option in SURFEXv8-Part 1: Model description, Geosci. Model Dev., 10, 843-872, 10.5194/gmd-10-843-2017, 2017.

Durot, K., Modélisation hydrologique distribuée du bassin versant nivo-pluvial de Sarennes. Validation des données d'entrées et développement d'un module de fonte nivale sous forêt, PhD. thesis, Laboratoire d'Etude des Transferts en Hydrologie et Environnement, UJF, 332 pp.., 1999.

Ellis, C. R., Pomeroy, J. W., and Link, T. E.: Modeling increases in snowmelt yield and desynchronization resulting from forest gap-thinning treatments in a northern mountain headwater basin, Water Resources Research, 49, 936-949, 10.1002/wrcr.20089, 2013.

Elzinga, C., Shearer, R. C., and Elzinga, G.: Observer Variation in Tree Diameter Measurements, Western Journal of Applied Forestry, 20, 134-137, 10.1093/wjaf/20.2.134, 2005.

Essery, R.: Large-scale simulations of snow albedo masking by forests, Geophysical Research Letters, 40, 5521-5525, 2013.

Essery, R., Bunting, P., Rowlands, A., Rutter, N., Hardy, J., Melloh, R., Link, T., Marks, D., and Pomeroy, J.: Radiative transfer modeling of a coniferous canopy characterized by airborne remote sensing, J. Hydrometeorol., 9, 228-241, 2008.

Essery, R., Rutter, N., Pomeroy, J., Baxter, R., Stahli, M., Gustafsson, D., Barr, A., Bartlett, P., and Elder, K.: An Evaluation of Forest Snow Process Simulations, Bull. Amer. Meteorol. Soc., 90, 1120-1136, 10.1175/2009bams2629.1, 2009.

Gouttevin, I., Lehning, M., Jonas, T., Gustafsson, D., and Molder, M.: A two-layer canopy model with thermal inertia for an improved snowpack energy balance below needleleaf forest (model SNOWPACK, version 3.2.1, revision 741), Geosci. Model Dev., 8, 2379-2398, 10.5194/gmd-8-2379-2015, 2015.

Halldin, S., and A. Lindroth: Errors in Net Radiometry: Comparison and Evaluation of Six Radiometer Designs, Journal of Atmospheric and Oceanic Technology, 9(6), 762-783, 1992.

Helbig, N., Moeser, D., Teich, M., Vincent, L., Lejeune, Y., Sicart, J. E., and Monnet, J. M.: Snow processes in mountain forests: interception modeling for coarse-scale applications, Hydrology and Earth System Sciences, 24, 2545-2560, 10.5194/hess-24-2545-2020, 2020.

Hojatimalekshah, A., Uhlmann, Z., Glenn, N. F., Hiemstra, C. A., Tennant, C. J., Graham, J. D., Spaete, L., Gelvin, A., Marshall, H. P., McNamara, J. P., and Enterkine, J.: Tree canopy and snow depth relationships at fine scales with terrestrial laser scanning, The Cryosphere, 15, 2187-2209, 10.5194/tc-15-2187-2021, 2021.

Jonas, T., Webster, C., Mazzotti, G., and Malle, J.: HPEval: A canopy shortwave radiation transmission model using high-resolution hemispherical images, Agric. For. Meteorol., 284, 9, 10.1016/j.agrformet.2020.107903, 2020.

Lejeune, Y., Dumont, M., Panel, J.-M., Lafaysse, M., Lapalus, P., Le, E., Gac, B. L., and Morin, S.: 57 years (1960-2017) of snow and meteorological observations from a mid-altitude mountain site (Col de Porte, France, 1325 m alt.), Earth System Science Data Discussions, 2018, 1-25, 2019.

López-Moreno, J. I., Leppänen, L., Luks, B., Holko, L., Picard, G., Sanmiguel-Vallelado, A., Alonso-González, E., Finger, D. C., Arslan, A. N., and Gillemot, K.: Intercomparison of measurements of bulk snow density and water equivalent of snow cover with snow core samplers: Instrumental bias and variability induced by observers, Hydrological Processes, 34, 3120-3133, 2020.

Lundquist, J. D., Dickerson-Lange, S. E., Lutz, J. A., & Cristea, N. C.: Lower forest density enhances snow retention in regions with warmer winters: A global framework developed from plot-scale observations and modeling. Water Resources Research, 49(10), 6356-6370, 2013.

Luoma, V., Saarinen, N., Wulder, M. A., White, J. C., Vastaranta, M., Holopainen, M., and Hyyppä, J.: Assessing Precision in Conventional Field Measurements of Individual Tree Attributes, Forests, 8, 38, 2017.

Malle, J., Rutter, N., Mazzotti, G., and Jonas, T.: Shading by Trees and Fractional Snow Cover Control the Subcanopy Radiation Budget, Journal of Geophysical Research: Atmospheres, 124, 3195-3207, 10.1029/2018jd029908, 2019.

Mazzotti, G., Essery, R., Moeser, C. D., and Jonas, T.: Resolving Small-Scale Forest Snow Patterns Using an Energy Balance Snow Model With a One-Layer Canopy, Water Resources Research, 56, e2019WR026129, https://doi.org/10.1029/2019WR026129, 2020.

Mazzotti, G., Currier, W. R., Deems, J. S., Pflug, J. M., Lundquist, J. D., and Jonas, T.: Revisiting Snow Cover Variability and Canopy Structure Within Forest Stands: Insights From Airborne Lidar Data, Water Resources Research, 55, 6198-6216, 10.1029/2019wr024898, 2019.

Michel, D., et al.: Performance and uncertainty of CNR1 net radiometers during a one-year field comparison, Journal of Atmospheric and Oceanic Technology, 25(3), 442-451, 2008.

Morin, S., Lejeune, Y., Lesaffre, B., Panel, J. M., Poncet, D., David, P., and Sudul, M.: An 18-yr long (1993-2011) snow and meteorological dataset from a mid-altitude mountain site (Col de Porte, France, 1325m alt.) for driving and evaluating snowpack models, Earth Syst. Sci. Data, 4, 13-21, 10.5194/essd-4-13-2012, 2012.

Musselman, K. N., Molotch, N. P., Margulis, S. A., Lehning, M., and Gustafsson, D.: Improved snowmelt simulations with a canopy model forced with photo-derived direct beam canopy transmissivity, Water Resources Research, 48, 2012.

Nobis, M., and U. Hunziker: Automatic thresholding for hemispherical canopy-photographs based on edge detection, Agricultural and Forest Meteorology, 128(3–4), 243-250,10.1016/j.agrformet.2004.10.002, 2005.

Otterman, J., Staenz, K., Itten, K. I., and Kukla, G.: Dependence of Snow Melting and Surface-Atmosphere Interactions on the Forest Structure, Bound.-Layer Meteor., 45, 1-8, 10.1007/bf00120812, 1988.

Philipona, R., et al.: Atmospheric longwave irradiance uncertainty: Pyrgeometers compared to an absolute sky-scanning radiometer, atmospheric emitted radiance interferometer, and radiative transfer model calculations, Journal of Geophysical Research-Atmospheres, 106(D22), 28129-28141, 2001.

Picard, G., Arnaud, L., Panel, J. M., and Morin, S.: Design of a scanning laser meter for monitoring the spatio-temporal evolution of snow depth and its application in the Alps and in Antarctica, The Cryosphere, 10, 1495-1511, 2016.

Pomeroy, J., Rowlands, A., Hardy, J., Link, T., Marks, D., Essery, R., Sicart, J. E., and Ellis, C.: Spatial Variability of Shortwave Irradiance for Snowmelt in Forests, J. Hydrometeorol., 9, 1482-1490, 10.1175/2008jhm867.1, 2008.

Reid, T., Essery, R., Rutter, N., and King, M.: Data-driven modelling of shortwave radiation transfer to snow through boreal birch and conifer canopies, Hydrological Processes, 28, 2987-3007, 2014.

Röhle, H.: Vergleichende Untersuchungen zur Ermittlung der Genauigkeit bei der Ablotung von Kronenradien mit dem Dachlot und durch senkrechtes Anvisieren des Kronenrandes (Hochblick-Methode), Forstarchiv, 57 (1), pp. 67-71, 1986.

Rutter, N., Essery, R., Pomeroy, J., Altimir, N., Andreadis, K., Baker, I., Barr, A., Bartlett, P., Boone, A., Deng, H. P., Douville, H., Dutra, E., Elder, K., Ellis, C., Feng, X., Gelfan, A., Goodbody, A., Gusev, Y., Gustafsson, D., Hellstrom, R., Hirabayashi, Y., Hirota, T., Jonas, T., Koren, V., Kuragina, A., Lettenmaier, D., Li, W. P., Luce, C., Martin, E., Nasonova, O., Pumpanen, J., Pyles, R. D., Samuelsson, P., Sandells, M., Schadler, G., Shmakin, A., Smirnova, T. G., Stahli, M., Stockli, R., Strasser, U., Su, H., Suzuki, K., Takata, K., Tanaka, K., Thompson, E., Vesala, T., Viterbo, P., Wiltshire, A., Xia, K., Xue, Y. K., and Yamazaki, T.: Evaluation of forest snow processes models (SnowMIP2), J. Geophys. Res.-Atmos., 114, 18, D06111, 10.1029/2008jd011063, 2009.

Sicart et al.: Snow Under Forest. Snow, forest and meteorological measurements at Col de Porte, SNOUF-OSUG [data set], http://dx.doi.org/10.17178/SNOUF.2022, 2022.

Van den Broeke, M., et al.: Surface radiation balance in Antarctica as measured with automatic weather stations, Journal of Geophysical Research, 109(D09103), doi:10.1029/2003JD004394, 2004.

Vincent, L.: Observation et modélisation du manteau neigeux sous une forêt d'épicéas au Col de Porte, Thèse de Master 2, Université Paul Sabatier, Toulouse, 40 pp., 2018.

Vionnet, V., Brun, E., Morin, S., Boone, A., Faroux, S., Le Moigne, P., Martin, E., and Willemet, J. M.: The detailed snowpack scheme Crocus and its implementation in SURFEX v7. 2, Geosci. Model Dev., 5, 773-791, 2012.

Webster, C., Rutter, N., Zahner, F., and Jonas, T.: Modeling subcanopy incoming longwave radiation to seasonal snow using air and tree trunk temperatures, Journal of Geophysical Research: Atmospheres, 121, 1220-1235, 2016.